Empirical modelling using dummy atoms (EMUDA): an alternative approach for studying "auxetic" structures

J. N. Grima[a]; R. Gatt[a]; T. G. C. Bray[a]; A. Alderson[b]; K. E. Evans[c]
[a] Department of Chemistry, University of Malta, Msida, Malta [b] Centre for Materials Research and Innovation, University of Bolton, Bolton, UK [c] Department of Engineering, University of Exeter, Exeter, UK

PLEASE SCROLL DOWN FOR ARTICLE

Empirical modelling using dummy atoms (EMUDA): an alternative approach for studying "auxetic" structures

J. N. GRIMA†*, R. GATT†, T. G. C. BRAY†, A. ALDERSON‡ and K. E. EVANS¶

†Department of Chemistry, University of Malta, Msida MSD 05, Malta
‡Centre for Materials Research and Innovation, University of Bolton, Bolton BL3 5AB, UK
¶Department of Engineering, University of Exeter, Exeter EX4 4QF, UK

Auxetics (materials or structures) are systems with a negative Poisson's ratio, a property that arises from the way various geometric features in the structure (or internal structure in the case of materials) deform when subjected to uniaxial loads. Such systems are normally studied by examining the behaviour of idealised representations of structures, which deform in a controlled fashion (e.g. deforming solely through hinging or stretching). Methods used for the analysis typically involve construction of real physical macro-models and/or derivation of analytical expressions for the mechanical properties. This paper proposes an alternative method for analysing such structures whereby idealised "hinging" or "stretching" structures are constructed within a molecular modelling environment using dummy atoms and examined using standard molecular mechanics techniques. We will show that this methodology of "empirical modelling using dummy atoms" (EMUDA) successfully reproduces the known properties of 2D conventional and auxetic hexagonal honeycombs hence confirming the suitability of this technique for studying auxetic structures.

1. Introduction

The Poisson's ratio is one of the fundamental mechanical properties of materials and describes the changes in shape that result when a material is uniaxially loaded. Mathematically, the Poisson's ratio of a material in a particular Ox_i–Ox_j plane for loading in the Ox_i direction is defined by [1]:

$$\nu_{ij} = -\frac{\text{strain in the orthogonal } Ox_j \text{ direction}}{\text{strain in the axial } Ox_i \text{ direction}} = -\frac{\varepsilon_j}{\varepsilon_i} \quad (1)$$

This property has a positive value in conventional materials since they contract when pulled (i.e. $-$ve ε_j and $+$ve ε_i) and expand when compressed (i.e. $+$ve ε_j and $-$ve ε_i). However, the theory of elasticity states that Poisson's ratios can also assume negative values, a property referred to as auxetic behaviour [2] which relates to materials that become wider when stretched and thinner when compressed. In fact, the theory of elasticity suggests that isotropic 3D materials may exhibit Poisson's ratios within the range $-1 \leq \nu \leq +1/2$ [1]; 2D isotropic

systems [3] can exhibit Poisson's ratios within the range $-1 \leq \nu \leq +1$; whilst there are no limits on the Poisson's ratios for anisotropic materials.

Negative Poisson's ratios are known to result in many beneficial enhancements in the properties of materials such as an increased resistance to indentation [4,5], and improved acoustic absorption properties [6,7]. These benefits make auxetic materials superior to conventional ones for various practical applications, with the result that there is considerable effort aimed at discovering new materials that exhibit auxetic behaviour. In fact, in recent years, auxetic behaviour has been predicted and/or experimentally measured in various types of materials including foams [8–12], nano- and micro-structured polymers [2,13–19], cubic metals [20], silicates [21–26] and zeolites [27]. In all of these materials, the negative Poisson's ratios can be explained in terms of the materials' particular nanostructure (in the case of the nanostructured polymers, metals, silicates and zeolites) or microstructure (in the case of the microstructured polymers and foams) and the way these nano/micro-structures deform when the materials are subjected to uniaxial loads. An important

*Corresponding author. E-mail: joseph.grima@um.edu.mt; URL: www.http//home.um.edu.mt/auxetic

feature that has emerged from the research in this field is that the Poisson's ratio is a scale-independent property [4]. In other words, the deformations can take place at the nano (molecular), micro or even at the macro level as the only requirement for auxetic behaviour is the right combination of the "geometry" and the "deformation mechanism". In view of this, a very popular approach for studying auxetic systems is to study "idealised structures" which could represent an idealised form of the nano/micro-structure of a material. These idealised structures can be studied mathematically by deriving analytical equations for their "mechanical properties" in terms of various geometric and structural parameters. Although, these analytical equations are sometimes tedious to derive, once available they provide researchers with a very important tool for gaining information about the behaviour of these structures and, more importantly, insight into the behaviour of the real materials which have nano/micro structures that are similar to these "idealised structures".

Here we propose an alternative method to deriving analytical equations for studying "idealised structures"—a method where the "structures" are constructed using "dummy atoms" and then modelled using custom-made force-fields within a commercially available molecular modelling package. This approach of "empirical modelling using dummy atoms" (EMUDA in short) will be tested on systems that have already been extensively studied through analytical modelling (the hexagonal honeycomb structure [28–31]) in an attempt to validate the EMUDA methodology.

2. The mechanical properties of hexagonal honeycomb structures

Hexagonal honeycomb structures deforming solely through hinging of the cell walls (the idealised hinging model) or solely through stretching of the cell walls (the idealised stretching model) have been extensively studied in view of their potential of exhibiting auxetic behaviour [28–31]. Referring to figure 1, it has been shown through analytical modelling that these systems
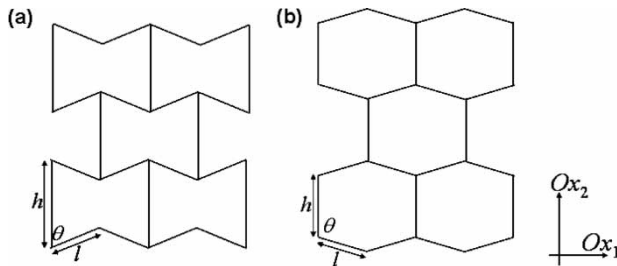

Figure 1. The (a) re-entrant; and (b) non re-entrant hexagonal honeycombs made from rod elements of lengths h and l at an angle θ to each other. Note that in the EMUDA models, the axes Ox_1 and Ox_2 will be set parallel to the Y and Z axes, respectively.

can exhibit both auxetic and conventional behaviour, and the sign of the Poisson's ratios depends on both the shape of the honeycomb and the deformation mechanisms:

(a) for $0 < \theta < 90°$ (i.e. for the re-entrant honeycombs):

$$\nu_{12}^{\text{hinging}}, \nu_{21}^{\text{hinging}} = -\text{ve} \quad \text{(auxetic behaviour)}$$

$$\nu_{12}^{\text{stretching}}, \nu_{21}^{\text{stretching}} = +\text{ve} \quad \text{(conventional behaviour)}$$

(b) for $90 < \theta < 180°$ (i.e. for the non re-entrant honeycombs):

$$\nu_{12}^{\text{hinging}}, \nu_{21}^{\text{hinging}} = +\text{ve} \quad \text{(conventional behaviour)}$$

$$\nu_{12}^{\text{stretching}}, \nu_{21}^{\text{stretching}} = -\text{ve} \quad \text{(auxetic behaviour)}$$

In fact, for the systems shown in figure 1, the strains in the Ox_i directions ($i = 1,2$) for the hinging and stretching modes of deformation are given by:

$$\varepsilon_i^{\text{hinging}} = \frac{1}{X_i}\frac{\mathrm{d}X_i}{\mathrm{d}\theta}\mathrm{d}\theta \quad \text{and} \quad \varepsilon_i^{\text{stretching}} = \frac{1}{X_i}\frac{\mathrm{d}X_i}{\mathrm{d}l}\mathrm{d}l,$$

$$i = 1, 2 \tag{2}$$

where X_1 and X_2 are dimensions of the unit cell along the Ox_1 and Ox_2 directions which are given by:

$$X_1 = 2l\sin(\theta) \quad \text{and } X_2 = 2(h - l\cos(\theta)) \tag{3}$$

and the analytical equations for the on-axis Poisson's ratios (from equations (1)–(3)) and Young's moduli for these hexagonal honeycomb systems are given by [30,31]:

For the Hinging model:

$$\nu_{12}^{\text{hinging}} = \frac{1}{\nu_{21}^{\text{hinging}}} = -\frac{\varepsilon_2^{\text{hinging}}}{\varepsilon_1^{\text{hinging}}} = -\tan(\theta)\frac{X_1}{X_2} \tag{4}$$

$$E_1^{\text{hinging}} = \frac{K_h}{bl^2\cos^2(\theta)}\frac{X_1}{X_2} \quad \text{and}$$

$$E_2^{\text{hinging}} = \frac{K_h}{bl^2\sin^2(\theta)}\frac{X_2}{X_1} \tag{5}$$

For the Stretching model:

$$\nu_{21}^{\text{stretching}} = -\frac{\varepsilon_1^{\text{stretching}}}{\varepsilon_2^{\text{stretching}}} = \frac{\sin\theta\cos\theta}{2 + \cos^2\theta}\frac{X_2}{X_1} \quad \text{and}$$

$$\nu_{21}^{\text{stretching}} = -\frac{\varepsilon_1^{\text{stretching}}}{\varepsilon_2^{\text{stretching}}} = \frac{\sin\theta\cos\theta}{2 + \cos^2\theta}\frac{X_2}{X_1} \tag{6}$$

$$E_1^{\text{stretching}} = \frac{K_s}{b\sin^2(\theta)}\frac{X_1}{X_2} \quad \text{and}$$

$$E_2^{\text{stretching}} = \frac{K_s}{b(2 + \cos^2(\theta))}\frac{X_2}{X_1} \tag{7}$$

where X_1/X_2 is the ratio of the unit cell dimensions X_1 and X_2 which is given by:

$$\frac{X_1}{X_2} = \frac{2l\sin(\theta)}{2(h - l\cos(\theta))} = \frac{\sin(\theta)}{(h/l) - \cos(\theta)} \quad (8)$$

b is the thickness of the honeycombs in the third dimension; K_h is the hinging force constant governing the resistance to "hinging" of the "θ-hinges" defined in the usual way, i.e. $M = K_h\delta\theta$ where M is the magnitude of the moment applied to the arm and $\delta\theta$ is the angular displacement of the arm of the honeycomb; K_s is the stretching force constant governing the resistance to "stretching" of the elements of the honeycombs defined in the usual way, i.e. $F = K_s\delta s$, where F is the magnitude of the force applied along the length of a honeycomb element of length s and δs is the change in length of the element.

The equations confirm that the Poisson's ratios are independent of scale and depend only on the ratio the lengths of the honeycomb cell walls, h/l, the angle θ between the cell walls (i.e. the geometry of the honeycomb) and the type of deformation mechanism (i.e. whether the system deforms through "idealised hinging" or "idealised stretching"). The equations also suggest that the magnitudes of the Young's moduli depend on scale, i.e. on the magnitude of b and l, but there are no restrictions on the range of values these geometric parameters can take.

3. The EMUDA methodology

The lack of restrictions on the scale at which the idealised honeycombs can be constructed permits the construction of these "honeycomb structures" at any scale including the nanometre scale, where they can be modelled using force-field based molecular modelling packages such as *Cerius*[2]. In such an environment, these idealised systems can be constructed by inserting "dummy atoms" at the vertices of the honeycombs and connecting these by "bonds" that would represent the "ribs" of the honeycombs. In this particular case, an infinite sheet of a honeycomb system may be constructed within *Cerius*[2] through the use of periodic boundary conditions where one unit cell contains four dummy atoms as shown in figure 2.

The shape and size of the honeycomb may be controlled by adjusting the magnitude of the distances and angles between connected atoms. This can be done by first labelling the dummy atoms in such a way that the different lengths/angles in the system may be uniquely identified (in this particular case, referring to figure 2, the dummy atoms may be labelled using two different labels, A and B†) and then listing the variables that need to be monitored during the simulation. Referring to figures 1 and 2, in this particular case, these variables are:
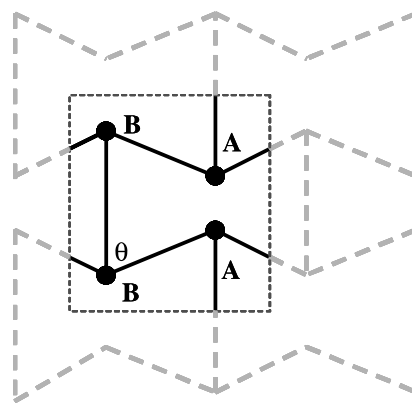

Figure 2. An EMUDA construct of the hexagonal honeycombs built from types of dummy atoms "A" and "B".

(1) the bond lengths |AA|, |BB| and |AB|, which for an unloaded honeycomb, their values should be equal to $|AA|_0 = |BB|_0 = h$ and $|AB|_0 = l$;
(2) the bond angles $|A\hat{A}B|$ and $|A\hat{B}B|$, which for an unloaded honeycomb, their values should be equal to $|A\hat{A}B|_0 = |A\hat{B}B|_0 = \theta$;
(3) the torsion angles ϕ between four connected atoms X–X–X–X, were X can be A or B, which must be set to 0 or $\pm 180°$ (a requirement for constraining the honeycomb system to stay planar).

The "rules" for describing the behaviour of these variables can now be coded in a custom-made force-field file that involves bond-terms but no VDW or coulombic interactions (or through the use of "restraints"). Such a force-field file must contain all the necessary information for setting up the "energy expression" of this "molecule" (or rather a "mechanical system" that obeys the classical laws of physics). In this particular case, an equation for the "potential energy" of the system can be written in the form [32]:

$$
\begin{aligned}
E = & \sum_{\text{all AB bonds}} \frac{1}{2}k_s\left(|AB| - |AB|_0\right)^2 \\
& + \sum_{\text{all AA bonds}} \frac{1}{2}k_s\left(|AA| - |AA|_0\right)^2 \\
& + \sum_{\text{all BB bonds}} \frac{1}{2}k_s\left(|BB| - |BB|_0\right)^2 \\
& + \sum_{\text{all ABB bond angles}} \frac{1}{2}k_h\left(|A\hat{B}B| - |A\hat{B}B|_0\right)^2 \\
& + \sum_{\text{all AAB bond angles}} \frac{1}{2}k_h\left(|A\hat{A}B| - |A\hat{A}B|_0\right)^2 \\
& + \sum_{\text{all X–X–X–X torsion angles}} \frac{1}{2}k_t[1 - \cos(2\phi)]
\end{aligned}
\quad (9)
$$

---

†It should be noted that the simplified labelling system using only two different "atom types" (A and B) as shown in figure 2b could be used since this simplified labelling system still permits the differentiation between the "bonds" of length l (i.e. bonds A–B) from the "bonds" of length h (i.e. bonds A–A and B–B) whilst all the A–B–B and A–A–B bond angles refer to θ-angles.

where the "spring constants" k_s, k_h and k_t define the resistance to "stretching" (i.e. changes in bond lengths), "hinging" (i.e. changes in bond angles), and "going out of plane", respectively. Since, the honeycomb systems are required to remain planar, k_t must be set as high as possible. Furthermore, it is possible to make the "stretching" or "hinging" mechanism predominate by setting $k_h \gg k_s$ (for systems deforming primarily through stretching of the "ribs" (i.e. stretching of the "bonds")), or by setting $k_s \gg k_h$ (for systems deforming primarily through hinging of the "θ-hinges").

Having set up the energy expression, the structures can be optimised ("minimised") using one of the minimisation algorithms in the modelling package so as to obtain the conformation with the lowest energy where the various bond lengths and angles will become equal, or as close as possible, to their respective ideal values that are defined in the force-field. The mechanical properties of the system can then be simulated using standard techniques for simulating the mechanical properties of molecular systems [32]. In *Cerius*[2], this can be done in a number of ways, including by computing the stiffness matrix **C** and its inverse, the compliance matrix **S** from the second derivative of the energy expression since:

$$c_{ij} = \frac{1}{V} \frac{\partial^2 E}{\partial \varepsilon_i \partial \varepsilon_j} \quad i, j = 1, 2, \ldots, 6, \qquad (10)$$

where V is the volume of the unit cell and ε_i are strain components. Other mechanical properties (including the on- and off-axis Poisson's ratios) can then be calculated from these matrices. Furthermore these periodic systems can be minimised with externally applied uniaxial stresses, a procedure that is particularly useful for the visualisation of the deformations in the structure that result from an externally applied uniaxial load.

4. Testing of the EMUDA methodology through modelling of various "idealised hinging" or "idealised stretching" honeycombs

4.1 Methods used

The simulations were performed using *Cerius*[2] V3.0 (Molecular Simulations Inc., San Diego, USA) on an O2 R5000 SGI workstation and involved: (a) the construction of the unminimised honeycomb structure within the molecular modelling environment; (b) writing of the custom-made force-field files; and (c) the calculations, i.e.

the simulation of the minimum energy structure and the calculation of the mechanical properties.

4.1.1 Construction of the unminimised model. An "unminimised" honeycomb model was constructed through the graphical interface and the "Crystal Builder" module of *Cerius*[2] using four dummy atoms per unit cell, which were assigned force-field types "A" and "B" as illustrated in figure 2. The honeycomb was aligned along the YZ-plane (that contains the (100) plane of the unit cell) with "bonds" of length h aligned parallel to the Z-axes (that corresponds to the [001] direction). This construction results in an infinite number of tessellates of "honeycombs" down the X-direction, which were kept aligned with each other at a separation of 1 Å during the simulation. This was done by constraining the unit cell parameters a, β and γ to remain "fixed" during the simulation at 1 Å, 90° and 90°, respectively, whilst allowing b, c and α to vary.

4.1.2 Construction of the custom-made force-field files. Twelve different force-field files were constructed with different combinations of (h, l), (k_h, k_s) and θ as listed in table 1. These force-field files describe honeycomb structures that deform solely, (in practice predominantly), through hinging of the θ-angles or through stretching of the "bonds" (the honeycomb ribs), where, referring to table 1, the force-field files with $(k_h, k_s) = (50 \,\text{kcal mol}^{-1}\text{rad}^{-2}, 10{,}000 \,\text{kcal mol}^{-1}\text{Å}^{-1})$ were designed to describe the "idealised hinging structures", since $k_h \ll k_s$, whilst the force-field files with $(k_h, k_s) = (10{,}000 \,\text{kcal mol}^{-1}\text{rad}^{-2}, 50 \,\text{kcal mol}^{-1}\text{Å}^{-2})$ were designed to describe the "idealised stretching structures", since $k_h \gg k_s$. In all simulations, k_t was set at the maximum value permitted by the software (999 kcal mol^{-1}).

Note that to avoid cumbersome conversion factors, the "stiffness constants" will be given in kcal mol^{-1} rad^{-2} (for angles) or kcal mol^{-1} Å^{-2} (for lengths), while lengths will be given in Å. The units of the stiffness constants relate to one mole ($N_A = 6.022 \times 10^{23}$) of angles or lengths, and can be converted to SI units through the conversion factors listed in Appendix I.

4.1.3 Calculations. For each of these 12 force-field files, the unminimised structure was first minimised using the SMART minimiser up to the default *Cerius*[2] high convergence criteria, which includes a condition that the RMS force must be less than 0.001 kcal mol^{-1} Å^{-1}. The numerical values of the mechanical properties were

Table 1.   Note that $|AA|_0 = |BB|_0 = h$, $|AB|_0 = l$ and $|A\hat{A}B|_0 = |A\hat{B}B|_0 = \theta$.

Parameters in equation (5)	Values used
(h, l)	(2Å, 1 Å)
(k_h, k_s)	$(50 \,\text{kcal mol}^{-1}\text{rad}^{-2}, 10{,}000 \,\text{kcal mol}^{-1}\text{Å}^{-2})$ or $(10{,}000 \,\text{kcal mol}^{-1}\text{rad}^{-2}, 50 \,\text{kcal mol}^{-1}\text{Å}^{-2})$
θ	30, 45 or 60° (for re-entrant honeycombs) 120, 135 or 150° (for non re-entrant honeycombs)

Table 2. The CPU time and the on-axis Poisson's ratios and Young's moduli for the "idealised hinging model" and the "idealised stretching model" with $\theta = 45°$, as predicted by the EMUDA model for different sizes of the unit cell relative to the smallest unit cell containing four "dummy atoms". Note that despite the differences in the CPU times, the properties of the systems with different unit cell sizes compare very well with each other and the values predicted by the analytical models (AM).

Mechanism	Type	$E_y = E_1$ (GPa)	$E_z = E_2$ (GPa)	$\nu_{yz} = \nu_{12}$	$\nu_{zy} = \nu_{21}$	CPU time (s)
Hinging	EMUDA (1 × 1)	752.58	2420.15	− 0.536	− 1.724	84
	EMUDA (2 × 2)	752.41	2419.56	− 0.536	− 1.724	106
	EMUDA (4 × 4)	752.45	2419.71	− 0.536	− 1.724	509
	AM	760.00	2540.31	− 0.547	− 1.828	n/a
Stretching	EMUDA (1 × 1)	379.10	253.99	0.544	0.365	71
	EMUDA (2 × 2)	379.04	253.94	0.544	0.365	106
	EMUDA (4 × 4)	379.04	253.94	0.544	0.365	480
	AM	379.93	254.03	0.547	0.366	n/a

calculated using the second derivative method. This produced the full 6 × 6 stiffness and compliance matrices. However, since the honeycombs are 2D systems aligned in the *YZ*-plane, only a sub-section of the full 6 × 6 stiffness and compliance matrices are of interest, namely the 3 × 3 sub-matrix, which relate solely to *Y*- and *Z*-directions. These 3 × 3 stiffness and compliance "sub-matrices" relate stress to strain for a 2D system in the *YZ*-plane and are defined through:

$$
\begin{pmatrix} \sigma_y \\ \sigma_z \\ \tau_{yz} \end{pmatrix} = \begin{pmatrix} c_{22} & c_{23} & c_{24} \\ c_{32} & c_{33} & c_{34} \\ c_{42} & c_{43} & c_{44} \end{pmatrix} \begin{pmatrix} \varepsilon_y \\ \varepsilon_z \\ \gamma_{yz} \end{pmatrix} \text{ and}
$$

$$
\begin{pmatrix} \varepsilon_y \\ \varepsilon_z \\ \gamma_{yz} \end{pmatrix} = \begin{pmatrix} s_{22} & s_{23} & s_{24} \\ s_{32} & s_{33} & s_{34} \\ s_{42} & s_{43} & s_{44} \end{pmatrix} \begin{pmatrix} \sigma_y \\ \sigma_z \\ \tau_{yz} \end{pmatrix},
$$

(11)

where the terms c_{ij} and s_{ij} in the 3 × 3 matrices refer to the respective terms in the original 6 × 6 matrices.

The Young's moduli E_y and E_z for loading in *Y*- and *Z*-directions, respectively, and the in-plane on-axis Poisson's ratios ν_{yz} and ν_{zy} for loading in *Y*- and *Z*-directions can be calculated from the terms in the compliance matrix, and are given by:

$$
E_y = \frac{\sigma_y}{\varepsilon_y} = \frac{1}{s_{22}} \quad E_z = \frac{\sigma_z}{\varepsilon_z} = \frac{1}{s_{33}}
$$

$$
\nu_{yz} = -\frac{\varepsilon_z}{\varepsilon_y} = -\frac{s_{32}}{s_{22}}
$$

(12)

$$
\nu_{zy} = -\frac{\varepsilon_y}{\varepsilon_z} = -\frac{s_{23}}{s_{33}}
$$

In addition to these second derivative calculations, minimisations of these systems at various uniaxially applied external loads were also performed in an attempt to "visualise" the effect of stress on the various geometric parameters of these systems.

Finally, it should be note that the unit cell used in these simulations, i.e. the one which contains only four atoms, is the smallest rectangular unit cell for such systems. In order to ensure that the quality of the results obtained were independent of the unit cell, a convergence test was carried out were a selection of the simulations were repeated with "superlattices" of (2 × 2) and (4 × 4) units containing 16 and 64 dummy atoms per unit cell, respectively.

4.2 Results and discussion:

All the "energy minimisations" and "second derivative calculations" with the smallest unit cells were observed to proceed to completion in less than two minutes on the SGI O2 workstation. However, the simulation time was considerably longer when the larger unit cells were used as illustrated in table 2. This increase in the computational time did not result in any significant differences in the values of the on-axis mechanical properties (see table 2, and hence it may be concluded that the smallest unit cell containing only four "dummy atoms" is a suitable representation for this infinite system for simulations of this type.

Images illustrating the deformations for a selection of the honeycombs as a result of the uniaxially applied loads are shown in figure 3 and in the supplementary information in electronic format (where they are shown as an animation). These images illustrate very clearly that the "hinging re-entrant" and the "stretching non re-entrant" honeycombs exhibit auxetic behaviour, whilst the "hinging non re-entrant" and the "stretching re-entrant" honeycombs exhibit conventional behaviour.

These observations are confirmed by the numerical values of the Poisson's ratios obtained from the second derivative method (table 3). A comparison of the simulated on-axis Poisson's ratios and Young's moduli with the equivalent values as predicted by the analytical models described in Section 2 suggests that the values of the Poisson's ratios and moduli simulated through the EMUDA method are generally in very close agreement with those predicted by the analytical models (within ± 3% in the case of the stretching models and within ± 11% in the case of the hinging models, see table 3). In this respect, it should be noted that the extent of agreement of the EMUDA simulated mechanical proper-
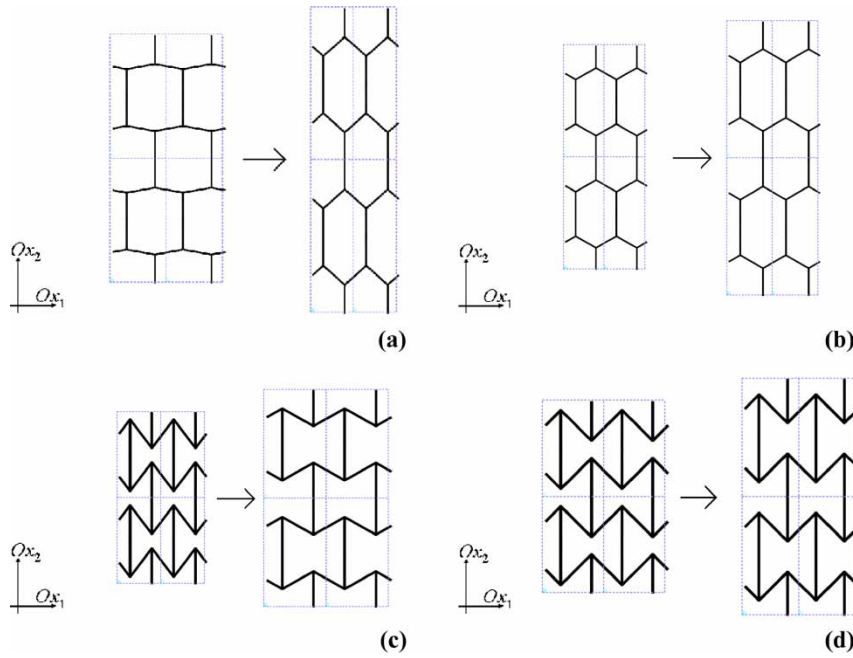
Figure 3.   The effect of loads on (a) a non re-entrant honeycomb deforming through hinging; (b) a non re-entrant honeycomb deforming through stretching; (c) a re-entrant honeycomb deforming through hinging, and (d) a re-entrant honeycomb deforming through stretching. (See animations.)

ties to those predicted by the analytical models is related to the magnitude of the Young's moduli (see figure 4), and in fact, the properties of the "stretching models" compared better with the analytical model than the "hinging models" as a result of the lower moduli of the "stretching models". This relationship between the "quality of the EMUDA results" and the moduli can be explained by the fact that an increase in the Young's modulus as predicted by the analytical expression of the idealised structures signifies that the structures are not easily deformed through the desired mode of deformation. In such scenarios, the assumption that the "desired mode of deformation" is the "predominant mode of deformation" can no longer be made as other modes of deformation start to compete effectively with the desired one.

In fact, one could argue that the scenarios studied here, i.e. where the honeycomb structures deform solely through "hinging" or through "stretching" represent unrealistic and highly idealised scenarios, as in reality, one would expect that there is superposition of effects given by stretching and hinging of the ribs†. In such systems, for loading by a stress σ_i in an Ox_i ($i = 1,2$) direction, the strains in the Ox_i direction are given by:

$$\varepsilon_i^{\text{stretching+hinging}} = \varepsilon_i^{\text{stretching}} + \varepsilon_i^{\text{hinging}} \qquad (13)$$

where $\varepsilon_i^{\text{stretching}}$ is the strain due to stretching and $\varepsilon_i^{\text{hinging}}$ is the strain due to hinging. But since a strain ε_i in an Ox_i direction is related to a stress σ_i in the same

direction through:

$$\varepsilon_i = \frac{1}{E_i} \sigma_i \qquad (14)$$

where E_i is the Young's modulus in the Ox_i direction, then from equations (13) and (14):

$$\frac{\sigma_i}{E_i^{\text{stretching+hinging}}} = \frac{\sigma_i}{E_i^{\text{stretching}}} + \frac{\sigma_i}{E_i^{\text{hinging}}} \qquad (15)$$

where $E_i^{\text{stretching+hinging}}$ is the Young's modulus in the Ox_i direction due to concurrent stretching and hinging, $E_i^{\text{stretching}}$ is the Young's modulus in the Ox_i direction due to stretching given by equation (7) whilst E_i^{hinging} is the Young's modulus in the Ox_i direction due to hinging given by equation (5).

By rearranging equation (15), the Young's modulus for loading in an Ox_i direction ($i = 1$, 2) for systems deforming through concurrent stretching and hinging is given by:

$$E_i^{\text{stretching+hinging}} = \frac{E_i^{\text{stretching}} E_i^{\text{hinging}}}{E_i^{\text{stretching}} + E_i^{\text{hinging}}} \qquad (16)$$

Furthermore, since from equation (1) the strain in the orthogonal Ox_j direction are given by:

$$\varepsilon_j = -\nu_{ji}\varepsilon_i = \frac{-\nu_{ji}}{E_i} \sigma_i \qquad (17)$$

and since in analogy to equation (13):

$$\varepsilon_j^{\text{stretching+hinging}} = \varepsilon_j^{\text{stretching}} + \varepsilon_j^{\text{hinging}} \qquad (18)$$

---

†In reality, one would also expect that the "rod elements" will "flex" to some extent, but the flexure mode of deformation [29] is not being included in these simulations due to the difficulty to represent flexure through the EMUDA methodology.

Table 3a. The on-axis Poisson's ratios and Young's moduli as predicted by the analytical model (AM) and as simulated by the EMUDA model, together with the deviations between these values.

θ (degrees)	Method	$E_y = E_1$ (GPa)	$E_z = E_2$ (GPa)	$\nu_{yz} = \nu_{12}$	$\nu_{zy} = \nu_{21}$
(A) Idealised hinging models					
30	AM	408.00	6301.91	−0.255	−3.928
	EMUDA	407.11	5678.19	−0.251	−3.504
	deviation	−0.22%	−9.90%	−1.32%	−10.81%
45	AM	760.00	2540.31	−0.547	−1.828
	EMUDA	752.45	2419.72	−0.536	−1.724
	deviation	−0.99%	−4.75%	−1.98%	−5.72%
60	AM	1604.00	1604.27	−1.000	−1.000
	EMUDA	1557.78	1557.80	−0.961	−0.961
	deviation	−2.88%	−2.90%	−3.88%	−3.88%
120	AM	963.00	2673.79	0.600	1.667
	EMUDA	934.67	2596.31	0.577	1.602
	deviation	−2.94%	−2.90%	−3.88%	−3.89%
135	AM	363.00	5318.99	0.261	3.828
	EMUDA	359.40	5067.11	0.256	3.610
	deviation	−0.99%	−4.74%	−1.99%	−5.71%
150	AM	162.00	15927.54	0.101	9.928
	EMUDA	161.11	14353.74	0.099	8.855
	deviation	−0.55%	−9.88%	−1.31%	−10.81%
(B) Idealised stretching models					
30	AM	612.60	286.45	0.764	0.357
	EMUDA	608.13	286.43	0.756	0.356
	deviation	−0.73%	−0.01%	−1.00%	−0.28%
45	AM	379.93	254.03	0.547	0.366
	EMUDA	379.04	253.94	0.544	0.365
	deviation	−0.23%	−0.04%	−0.50%	−0.30%
60	AM	267.38	267.38	0.333	0.333
	EMUDA	267.20	267.20	0.332	0.332
	deviation	−0.07%	−0.07%	−0.34%	−0.34%
120	AM	160.43	445.63	−0.200	−0.556
	EMUDA	160.32	445.34	−0.199	−0.554
	deviation	−0.07%	−0.07%	−0.35%	−0.33%
135	AM	181.45	531.9	−0.261	−0.766
	EMUDA	181.03	531.72	−0.260	−0.763
	deviation	−0.23%	−0.03%	−0.50%	−0.30%
150	AM	242.38	723.98	−0.302	−0.903
	EMUDA	240.64	723.86	−0.299	−0.900
	deviation	−0.72%	−0.02%	−0.98%	−0.28%

then from equations (17) and (18):

$$\frac{-\nu_{ij}^{\text{stretching+hinging}} \cdot \sigma_i}{E_i^{\text{stretching+hinging}}} = \frac{-\nu_{ij}^{\text{stretching}} \cdot \sigma_i}{E_i^{\text{stretching}}} + \frac{-\nu_{ij}^{\text{hinging}} \cdot \sigma_i}{E_i^{\text{hinging}}} \quad (19)$$

where $\nu_{ij}^{\text{stretching+hinging}}$ is the Poisson's ratio in the $Ox_i - Ox_j$ plane for loading in the Ox_i direction due to concurrent stretching and hinging, $\nu_{ij}^{\text{stretching}}$ is the Poisson's ratio in

Figure 4. The percentage differences (absolute values) of the Poisson's ratios from the EMUDA model when compared to the analytical model.

the $Ox_j - Ox_j$ plane for loading in the Ox_i direction due to stretching given by equation (6) whilst $\nu_{ij}^{\text{hinging}}$ is the Poisson's ratio in the $Ox_i - Ox_j$ plane for loading in the Ox_i direction due to hinging given by equation (4).

By rearranging equation (19), the Poisson's ratio in the $Ox_i - Ox_j$ plane for loading in the Ox_i direction $(i,j = 1, 2)$ for systems deforming through concurrent stretching and hinging is given by:

$$\nu_{ij}^{\text{stretching+hinging}} = \frac{\nu_{ij}^{\text{stretching}} E_i^{\text{hinging}} + \nu_{ij}^{\text{hinging}} E_i^{\text{stretching}}}{E_i^{\text{stretching}} + E_i^{\text{hinging}}}$$

$$(20)$$

In an attempt to assess the suitability of the EMUDA modelling technique for simulating such more realistic systems, the simulations described in section 4.1 were repeated with force constants $(k_h, k_s) = (50 \text{ kcal mol}^{-1} \text{rad}^{-2}, 50 \text{ kcal mol}^{-1} \text{Å}^{-2})$. As illustrated in table 4, the simulated values of the moduli and Poisson's ratios for these "concurrent stretching and hinging" systems compare extremely well with those predicted by
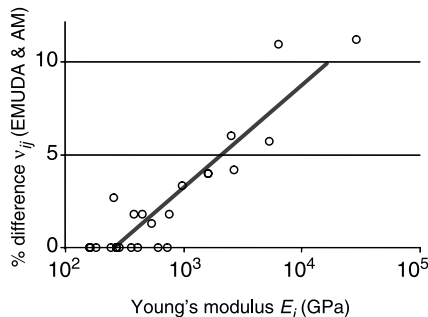
Table 4.   The on-axis Poisson's ratios and Young's moduli for the "hinging + stretching models" as predicted by the analytical model (AM) derived here and as simulated by the EMUDA model, together with the deviations between these values.

θ (degrees)	Method	$E_y = E_1$ (GPa)	$E_z = E_2$ (GPa)	$\nu_{yz} = \nu_{12}$	$\nu_{zy} = \nu_{21}$
30	AM	245.04	274.00	0.15274	0.17079
	EMUDA	245.08	274.04	0.15270	0.17080
	deviation	0.016%	0.016%	−0.027%	0.005%
45	AM	253.29	230.94	0.18231	0.16622
	EMUDA	253.35	231.18	0.18200	0.16610
	deviation	0.025%	0.105%	−0.168%	−0.073%
60	AM	229.18	229.18	0.14286	0.14286
	EMUDA	229.22	229.22	0.14290	0.14290
	deviation	0.016%	0.016%	0.030%	0.030%
120	AM	137.51	381.97	−0.08571	−0.23810
	EMUDA	137.53	382.03	−0.08570	−0.23810
	deviation	0.016%	0.016%	−0.017%	0.002%
135	AM	120.97	483.54	−0.08707	−0.34804
	EMUDA	120.64	483.61	−0.08690	−0.34850
	deviation	−0.269%	0.013%	−0.193%	0.133%
150	AM	96.95	692.50	−0.06043	−0.43166
	EMUDA	96.97	692.61	−0.06040	−0.43170
	deviation	0.016%	0.016%	−0.056%	0.009%

the analytical model derived here and given by equations (16) and (20) (within $\pm 1\%$, generally the EMUDA Poisson's ratios agree to the values of the analytical model to the 4th decimal place).

All this is very significant as it confirms that the EMUDA technique is suitable for simulating the mechanical properties of these structures, and in particular, it can be used easily and successfully to:

(1) assess whether a particular idealised structure constructed from "rods" deforming solely through "hinging" or "stretching" exhibits conventional or auxetic behaviour, and to what extent it does so;
(2) determine how changes in the geometric and structural characteristics affect the mechanical properties;
(3) visualise and measure the effect of stresses on the geometry of these structures and hence elucidate the "deformation mechanism/s"; and
(4) simulate more realistic systems constructed from "rods" which deform through "concurrent hinging and stretching" (i.e. it can simulate the superposition of effects given by stretching and hinging of the rods).

In other words, the EMUDA technique offers an excellent alternative to the construction of analytical expressions and/or real physical models that can be tedious, expensive and/or time consuming to derive or produce (especially by chemists who may be more familiar with molecular modelling techniques than with techniques relating to modelling of "structures"). In this respect, it should be noted that EMUDA models offer the advantage that they combine the strengths of physical models and analytical expression in the sense that like the analytical models (but unlike the real physical models), the EMUDA models can be very easily modified to study the effect of changes in the various structural characteristics (a new physical model would need to be constructed

for each modification introduced), and like the physical models (but unlike the analytical models) the EMUDA models allows the user to immediately and easily "visualise" the changes in the shape and size of the structure.

However, the real strength of this new technique is that it is not restricted to the study honeycomb systems and it may be used to simulate the properties of virtually any system composed from rods that deforms through hinging or stretching. This is very significant as it provides researchers with a quick, easy and inexpensive alternative for studying structures that could potentially exhibit negative Poisson's ratios. In this respect, it is important to note that the observation that the quality of simulated results improves as the Young's moduli are lowered suggests that when modelling novel systems, care should be taken that the parameters are chosen in such a way that the moduli are kept low. (For example, these simulations suggest that if the moduli of planar parallel systems arranged at 1 Å to each other in the *YZ*-plane are lower than 10^4 GPa, then the simulated properties will be accurate within $\pm 10\%$, see table 4. Note that these values of the moduli refer to planar parallel systems arranged at 1 Å to each other in the third direction).

It should also be noted that this work suggests that molecular modelling programs could be easily transformed into tools that may be used by architects and structural engineers for visualising and analysing structures/mechanisms and to understand how the structures behave when subjected to mechanical loads, in the same way that finite element (FE) modelling software normally used by engineers has been successfully used to model molecular systems (e.g. carbon single-walled nanotubes [33,34]). We hope that this will encourage software manufacturers to put more effort into the design of "molecular modelling packages" in view of the increased marketability of "modified versions" of these packages.

Table 5. The conversion factors required for comparing the EMUDA results with those predicted by the analytical model.

Parameter SI units (as used in analytical equation)	Parameter in the EMUDA model	Conversion factor	Calculated as . . .
h (m)	h (Å)	$\times\ 10^{-10}$	Å $\rightarrow$ m: $\times\ 10^{-10}$
l (m)	l (Å)	$\times\ 10^{-10}$	Å $\rightarrow$ m: $\times\ 10^{-10}$
K_h (J rad^{-2})	k_h (kcal mol^{-1} rad^{-2})	$\times\ 4184 N_A$	kcal $\rightarrow$ J: $\times\ 4.184 \times 10^3$
			"moles" $\rightarrow$ "units" : $\times N_A$
K_s (J m^{-2})	k_s (kcal mol^{-1} Å^{-2})	$\times\ 4184 N_A \times 10^{20}$	kcal $\rightarrow$ J: $\times\ 4.184 \times 10^3$
			"moles" $\rightarrow$ "units": $\times N_A$ Å^{-2} $\rightarrow$ m^{-2} $\div (10^{-10})^2$

5. Conclusions

This work has shown that the effect of mechanical loads on the shape of structures composed from rods that deform through relative changes of the angles between the rods (i.e. hinging of the rods) or stretching of the rods can be modelled using standard force-field based molecular modelling methods through a technique, which is being referred to as "EMUDA". It has also been shown that this EMUDA technique can reproduce the properties of conventional and auxetic hexagonal honeycombs deforming through stretching or hinging of the ribs of the honeycomb to an acceptable level of accuracy, which is dependent on the stiffness of the honeycombs. All this suggests that the EMUDA technique is likely to offer a very effective alternative for studying the properties of novel "auxetic" systems that very frequently are assumed to deform in such ways (i.e. through hinging or stretching) without the need of constructing more expensive real physical models or to derive analytical expressions for the Poisson's ratios, with the result that it will facilitate the discovery, analysis and development of new auxetic systems.

Acknowledgements

Appendix I

The units as used in the EMUDA simulations can be converted to SI to be compared with the analytical equations in Section 2 through the conversion factors given in Table 5.

References

[1] B.M. Lempriere. Poisson's ratio in orthotropic materials. *AIAA J.*, **6**, 2226 (1968).

[2] K.E. Evans, M.A. Nkansah, I.J. Hutchinson, S.C. Rogers. Molecular network design. *Nature*, **353**, 124 (1991).

[3] K.W. Wojciechowski. Remarks on "Poisson ratio beyond the limits of the elasticity theory". *J. Phys. Soc. Jpn.*, **72**, 1819 (2003).

[4] A. Alderson. A triumph of lateral thought. *Chem. Ind.*, **10**, 384 (1999).

[5] R.S. Lakes, K. Elms. Indentability of conventional and negative Poisson's ratio foams. *J. Compos. Mater.*, **27**, 1193 (1993).

[6] F. Scarpa, W.A. Bullough, P. Lumley. Trends in acoustic properties of iron particle seeded auxetic polyurethane foam. *P.I. Mech. Eng. C—J. Mech. Eng. Sci.*, **218**, 241 (2004).

[7] F. Scarpa, F.C. Smith. Passive and MR fluid-coated auxetic PU foam—Mechanical, acoustic, and electromagnetic properties. *J. Int. Mater. Syst. Struct.*, **15**, 973 (2004).

[8] R. Lakes. Foam structures with a negative Poisson's ratio. *Science*, **235**, 1038 (1987).

[9] K.E. Evans, M.A. Nkansah, I.J. Hutchinson. Auxetic foams—modeling negative Poisson's ratios. *Acta Metall. Mater.*, **42**, 1289 (1994).

[10] N. Gaspar, C.W. Smith, E.A. Miller, G.T. Seidler, K.E. Evans. Quantitative analysis of the microscale of auxetic foams. *Phys. State Solid (b)*, **242**, 550 (2005).

[11] C.W. Smith, J.N. Grima, K.E. Evans. A novel mechanism for generating auxetic behaviour in reticulated foams: Missing rib foam model. *Acta Mater.*, **48**, 4349 (2000).

[12] J.N. Grima, A. Alderson, K.E. Evans. An alternative explanation for the negative Poisson's ratios in auxetic foams. *J. Phys. Soc. Jpn.*, **74**, 1341 (2005).

[13] A.P. Pickles, K.L. Alderson, K.E. Evans. The effects of powder morphology on the processing of auxetic polypropylene (PP of negative Poisson's ratio). *Polym. Eng. Sci.*, **36**, 636 (1996).

[14] K.L. Alderson, K.E. Evans. Strain-dependent behavior of microporous polyethylene with a negative Poisson ratio. *J. Mater. Sci.*, **28**, 4092 (1993).

[15] K.E. Evans, B.D. Caddock. Microporous materials with negative poisson ratios .2. Mechanisms and interpretation. *J. Phys. D: Appl. Phys.*, **22**, 1877 (1989).

[16] J.N. Grima, J.J. Williams, K.E. Evans. Networked calix[4]arene polymers with unusual mechanical properties. *Chem. Commun.*, DOI 0.1039/b505839b (2005).

[17] J.N. Grima, K.E. Evans. Self expanding molecular networks. *Chem. Commun.*, **16**, 1531 (2000).

[18] R.H. Baughman, D.S. Galvao. Crystalline networks with unusual predicted mechanical and thermal-properties. *Nature*, **365**, 735 (1993).

[19] C.B. He, P.W. Liu, A.C. Griffin. Toward negative Poisson ratio polymers through molecular design. *Macromolecules*, **31**, 3145 (1998).

[20] R.H. Baughman, J.M. Shacklette, A.A. Zakhidov, S. Stafstrom. Negative Poisson's ratios as a common feature of cubic metals. *Nature*, **392**, 362 (1998).

[21] A. Yeganeh-Haeri, D.J. Weidner, J.B. Parise. Elasticity of alpha-cristobalite—a silicon dioxide with a negative Poisson's ratio. *Science*, **257**, 650 (1992).

[22] N.R. Keskar, J.R. Chelikowsky. Negative Poisson ratios in crystalline SiO$_2$ from 1st-principles calculations. *Nature*, **358**, 222 (1992).

[23] A. Alderson, K.L. Alderson, K.E. Evans, J.N. Grima, M. Williams. Modelling of negative Poisson's ratio nanomaterials: deformation mechanisms, structure–property relationships and applications. *J. Metastable Nanocryst. Mater.*, **23**, 55 (2005).

[24] A. Alderson, K.E. Evans. Rotation and dilation deformation mechanisms for auxetic behaviour in the alpha-cristobalite tetrahedral framework structure. *Phys. Chem. Miner.*, **28**, 711 (2001).

[25] A. Alderson, K.L. Alderson, K.E. Evans, J.N. Grima, M.R. Willams, P.J. Davies. Modelling the deformation mechanisms, structure-property relationships and applications of auxetic nanomaterials. *Phys. State Solid (b)*, **242**, 499 (2005).

[26] J.N. Grima, R. Gatt, A. Alderson, K.E. Evans. On the origin of auxetic behaviour in the silicate α-cristobalite. *J. Mater. Chem.*, DOI: 10.1039/b508098c (2005).

[27] J.N. Grima, R. Jackson, A. Alderson, K.E. Evans. Do zeolites have negative Poisson's ratios? *Adv. Mater.*, **12**, 1912 (2000).

[28] F.K. Abd el-Sayed, R. Jones, I.W. Burgens. Theoretical approach to the deformation of honeycomb based composite-materials. *Composites*, **10**, 209 (1979).

[29] L.J. Gibson, M.F. Ashby. *Cellular Solids: Structure and Properties*, Oxford, Pergamon, Oxford (1988).

[30] I.G. Masters, K.E. Evans. Models for the elastic deformation of honeycombs. *Compos. Struct.*, **35**, 403 (1996).

[31] K.E. Evans, A. Alderson, F.R. Christian. Auxetic 2D polymer networks—an example of tailoring geometry for specific mechanical—properties. *J. Chem. Soc. Faraday Trans.*, **91**, 2671 (1995).

[32] Cerius[2], *'Force-field Based Simulations' and 'Property prediction' User Guides*, Molecular Simulations Inc., San Diego (1997).

[33] C. Li, W. Chou. Elastic properties of single-walled carbon nanotubes in transverse directions. *Phys. Rev. B*, **69**, 073401 (2004).

[34] K.I. Tserpesa, P. Papanikos. Finite element modeling of single-walled carbon nanotubes. *Compos.: Part B*, **36**, 468 (2005).